Supplementary Figure 1

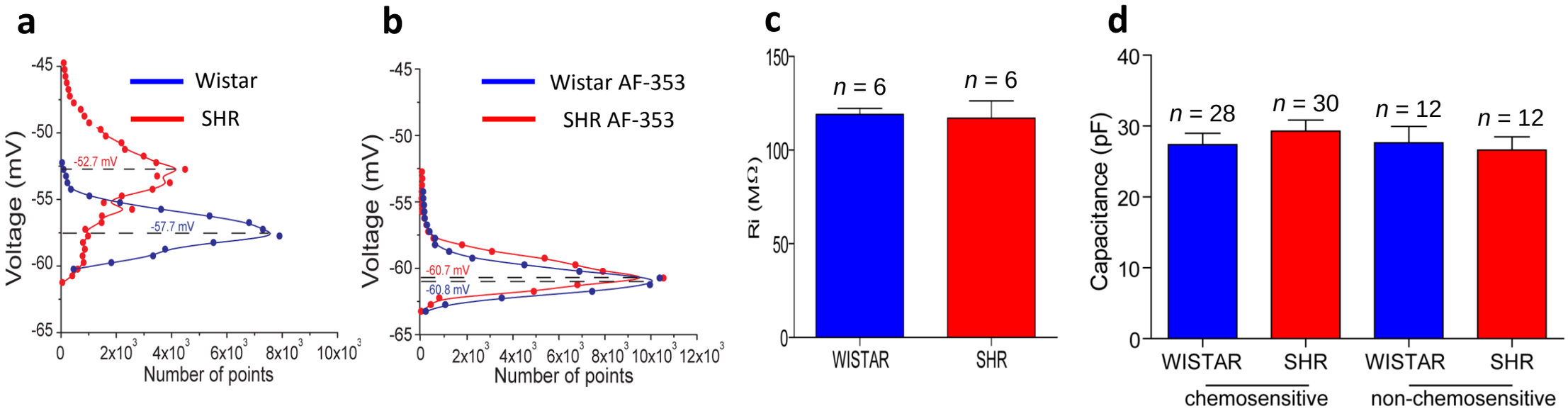

Supplementary Figure 1

Neurophysiological properties of petrosal chemoreceptive neurones in Wistar and SH rats. Control membrane potentials were measured from physiologically characterized chemoreceptive petrosal neurones at high sampling frequency and compared between rat strains before (**a**) and after AF-353 application to the CB ((**b**); 15 nl 20 μM, *n* = 10 or 11). The more depolarized potentials in SHR neurones ($P < 0.001$) was abolished after P2X3 receptor blockade. (**c**): There was no difference in membrane input resistance of petrosal chemoreceptive neurones between Wistar and SH rats. (**d**): No difference was found in petrosal membrane capacitance between Wistar and SHR for both chemoreceptive and non-chemoreceptive petrosal neurones.

Supplementary Figure 2

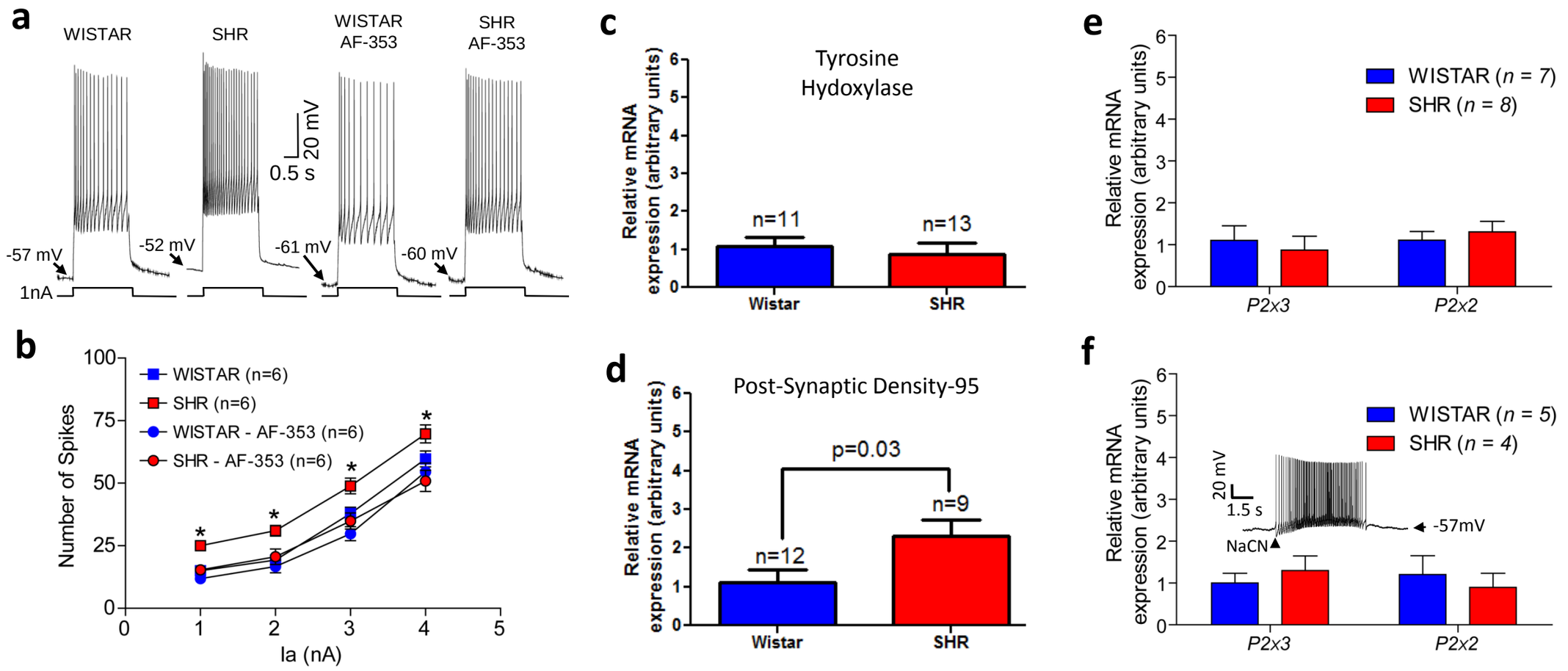

Supplementary Figure 2.

Chemoreceptive petrosal neurone characteristics in Wistar and SH rats. (**a)**, (**b**), The firing responses of chemoreceptive petrosal cells to injected current were more excitable in SH rats and this was reduced to levels seen in Wistar rats by blocking P2X3 receptors within the carotid body (not petrosal ganglia) with AF-353 microinfusion. (**c**), In chemoreceptive petrosal cells there was no difference in tyrosine hydroxylase (TH) mRNA between rat strains. (**d**), Post-synaptic density protein 95 (PSD-95) mRNA was upregulated in chemoreceptive petrosal cells of SH rats indicative of more synaptic contacts. (**e**), There was no difference in *P2x2* or *P2x3* receptor mRNA in non-chemoreceptive (unidentified) petrosal neurones between SH and Wistar rats. (**f**), There was no rat strain difference in mRNA of *P2x2* or *P2x3* receptors in identified chemoreceptive neurones located in the nucleus tractus solitarii.

Supplementary Figure 3

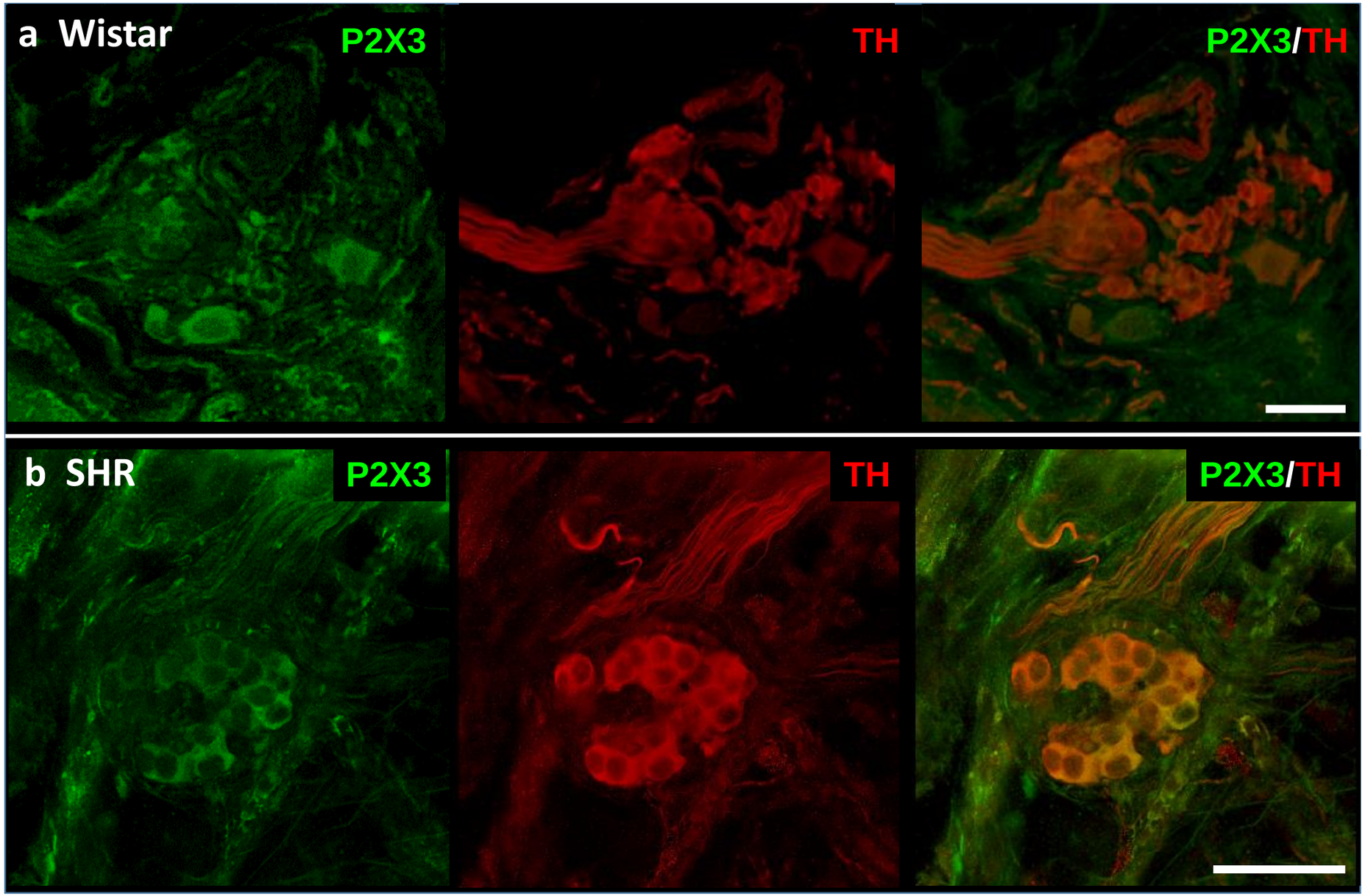

Supplementary Figure 3 P2X3 receptor and tyrosine hydroxylase (TH) immunofluorescence in the carotid body of rats. Note the P2X3 receptor expression in TH positive cells (glomus cells) and fibres were more evident in the SH rats (**b**) compared with Wistar rats (**a**). Scale bars 50 μm.

Supplementary Figure 4

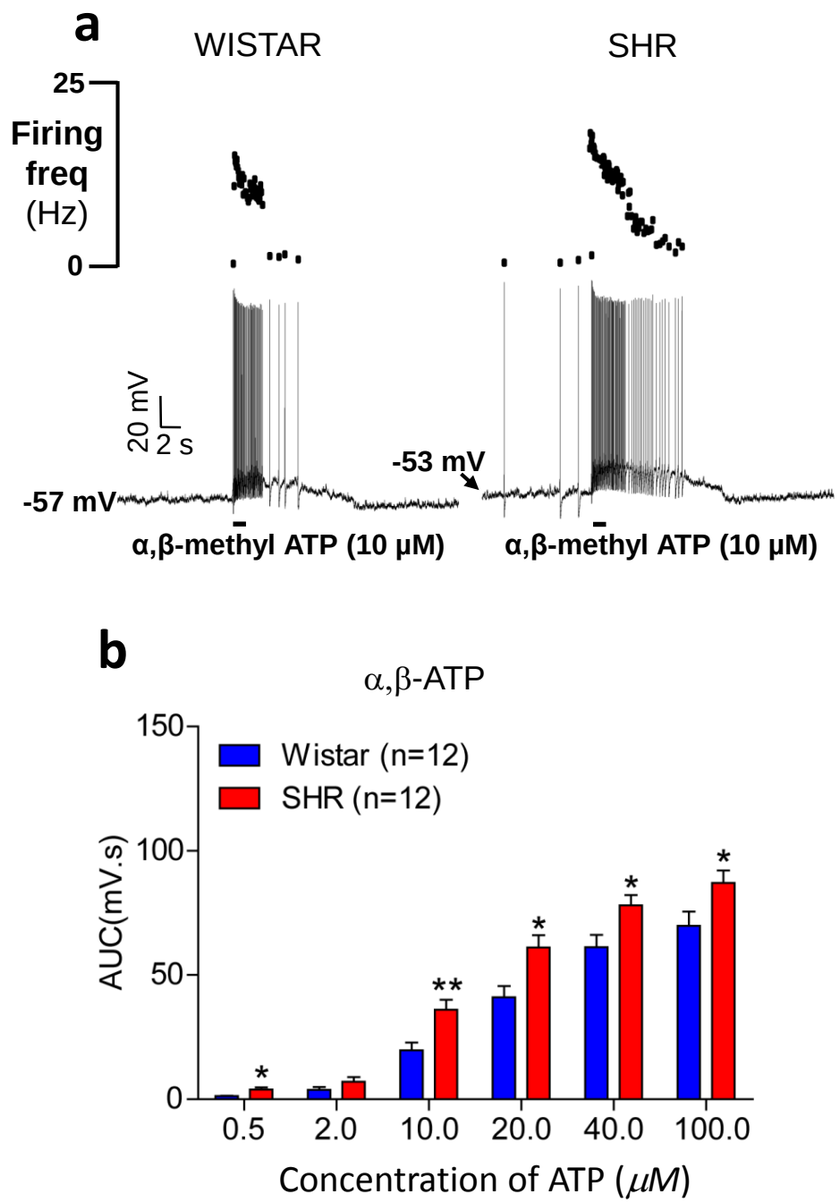

Supplementary Figure 4

Chemoreceptive petrosal neurone sensitivity to α-β-methylene ATP. In Wistar and SH rats The stable analogue of ATP (α-β-methylene ATP evoked greater firing responses (**a**) and membrane depolarisations (**b**) in chemoreceptive petrosal neurones from SH (n = 13) than Wistar rats (n = 10). All data from the *in situ* arterially perfused preparation. Unpaired t-test. AUC, area under the curve. *, $P < 0.05$.

Supplementary Figure 5

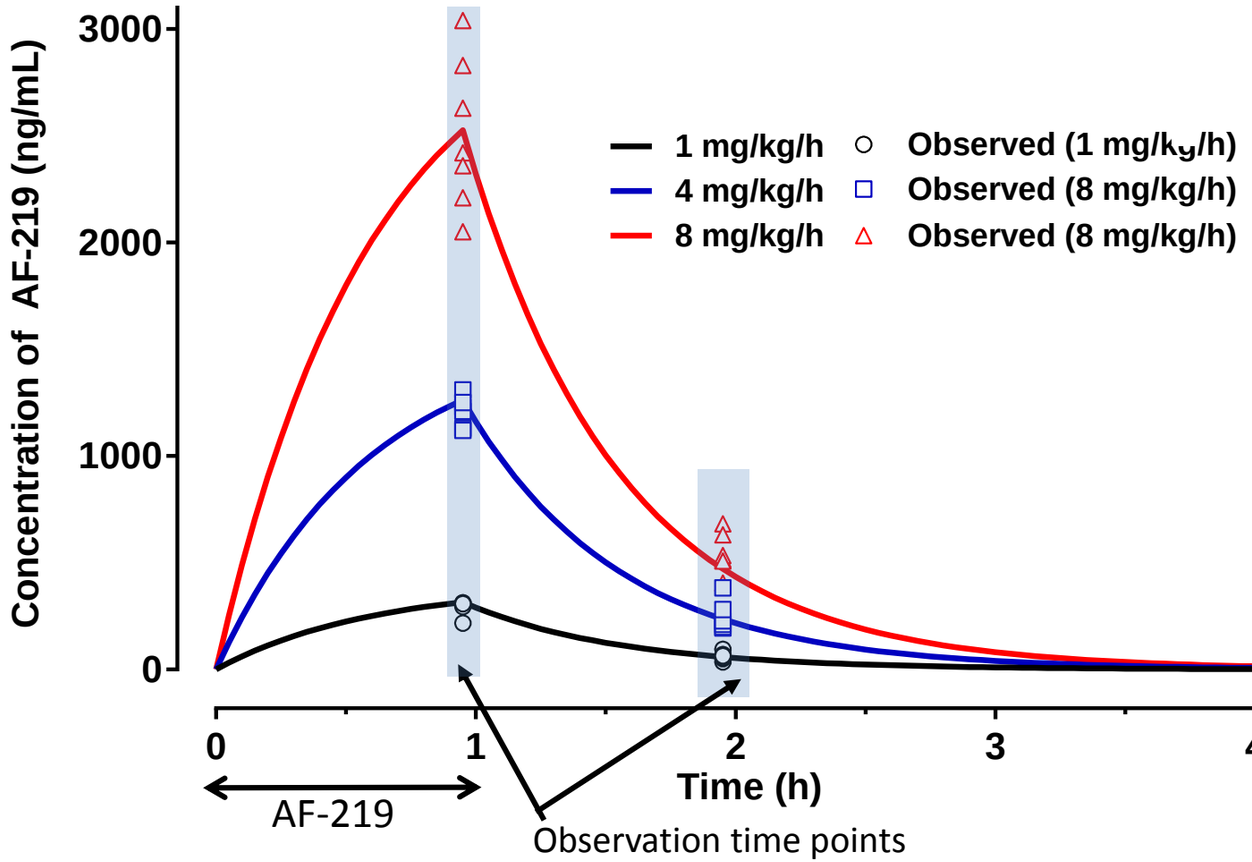

Supplementary Figure 5
Pharmacokinetic profile of AF-219 in rat plasma. The pharmacokinetic data are indicated by symbols for the three doses of AF219 (colour coded) infused i.v. into conscious rats (*n* = 7). Blood samples were taken at 60 and 120 minutes and highlighted by shaded blue areas. Solid lines represent modeled pharmacokinetic response to AF-219 at corresponding doses. Two rats were excluded from blood sampling due to technical issues with the venous line.

Supplementary Figure 6

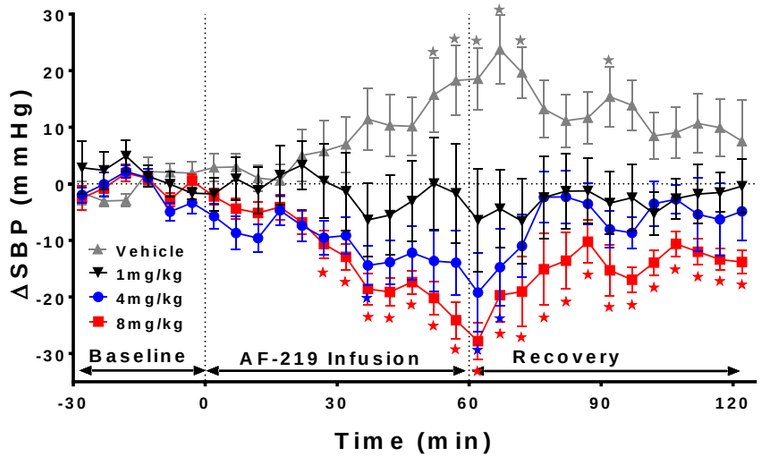

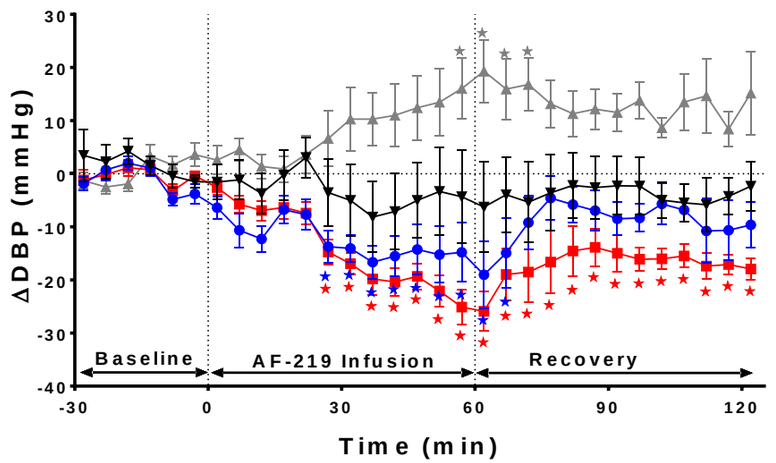

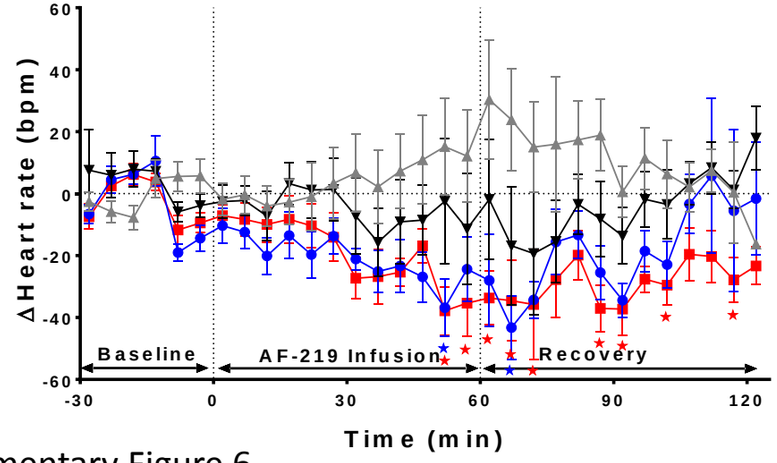

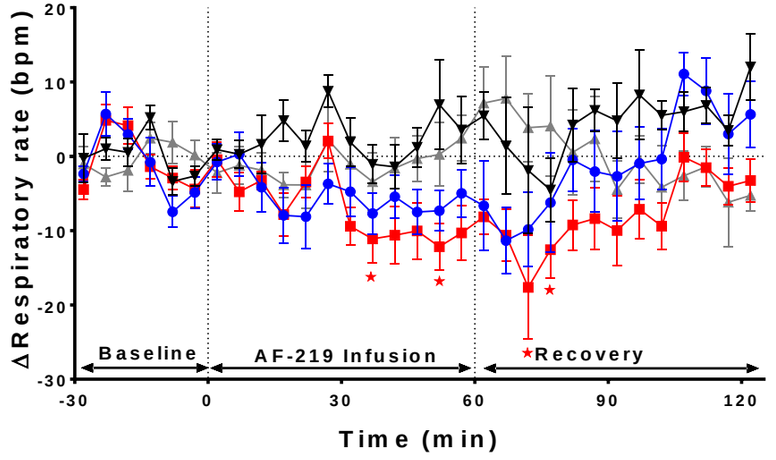

Supplementary Figure 6

Cardiovascular and respiratory response dynamics during infusion of AF-219 in SH rats. Time profile of the change in systolic blood pressure (SBP); diastolic blood pressure (DBP), heart rate and respiratory rate with Vehicle (grey), 1mg/kg/h (black); 4mg/kg/h (blue); 8 mg/kg/h (red) i.v. infusion of AF-219 in the SH rat (n = 7). Data are corrected for vehicle effect. * $P < 0.05$, one-way ANOVA with Dunnett's test. Data points were excluded if rats overtly started moving during the infusion period.

Supplementary Figure 7

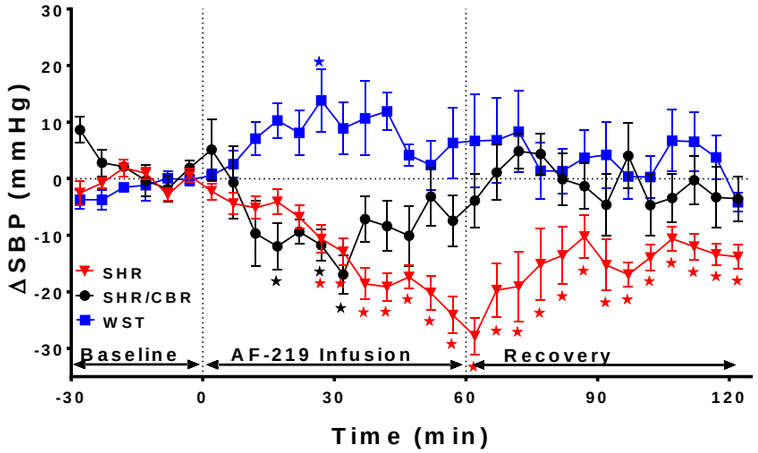

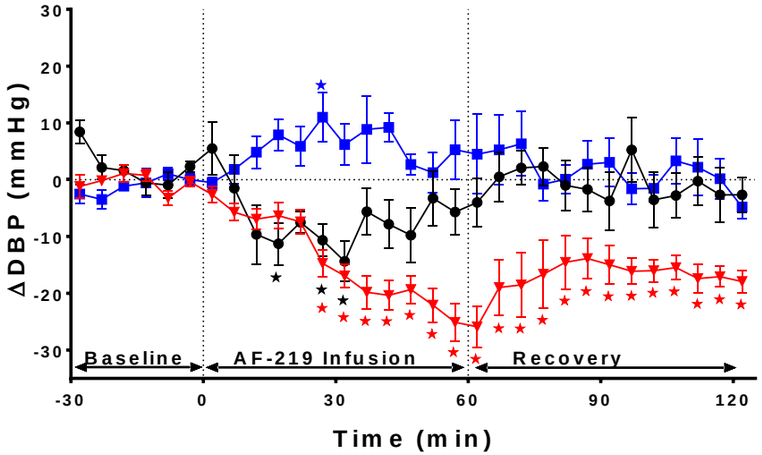

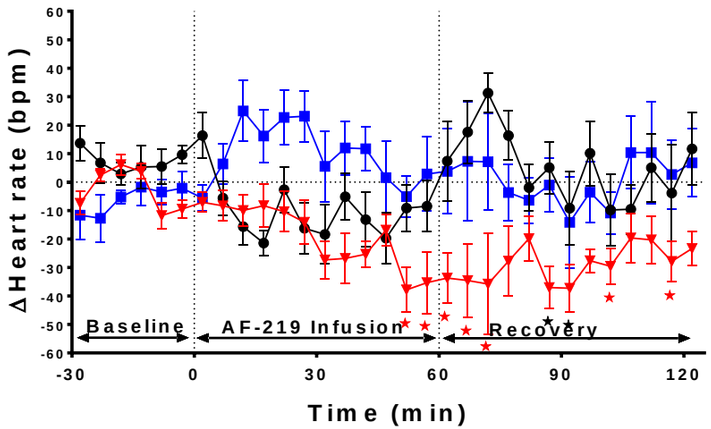

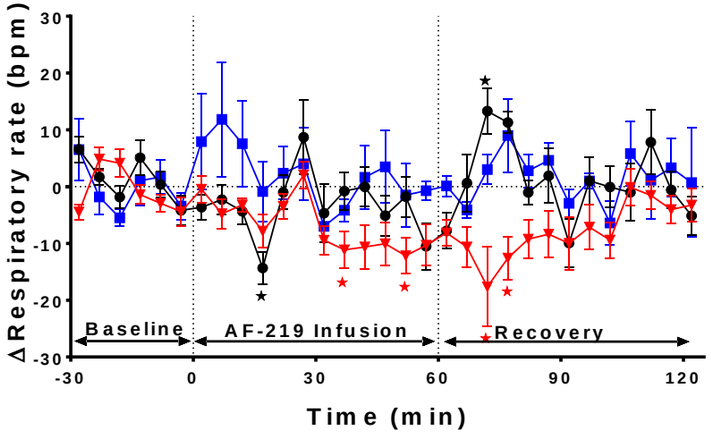

Supplementary Figure 7

Dependence on carotid body for the cardiovascular and respiratory responses following AF-219 infusion into SH rats. Time profile of the reduction in systolic blood pressure (SBP); diastolic blood pressure (DBP), heart rate and respiratory rate with 8 mg/kg/h i.v. infusion of AF-219 in the SH rats (n = 7) before and after selective carotid body resection (SHR/CBR). Note absence of response in the normotensive Wistar rat (n = 7). Data are corrected for vehicle effect, *, $P < 0.05$, one-way ANOVA with Dunnett's test. Data points were excluded if rats overtly started moving during the infusion period.

Supplementary Figure 8

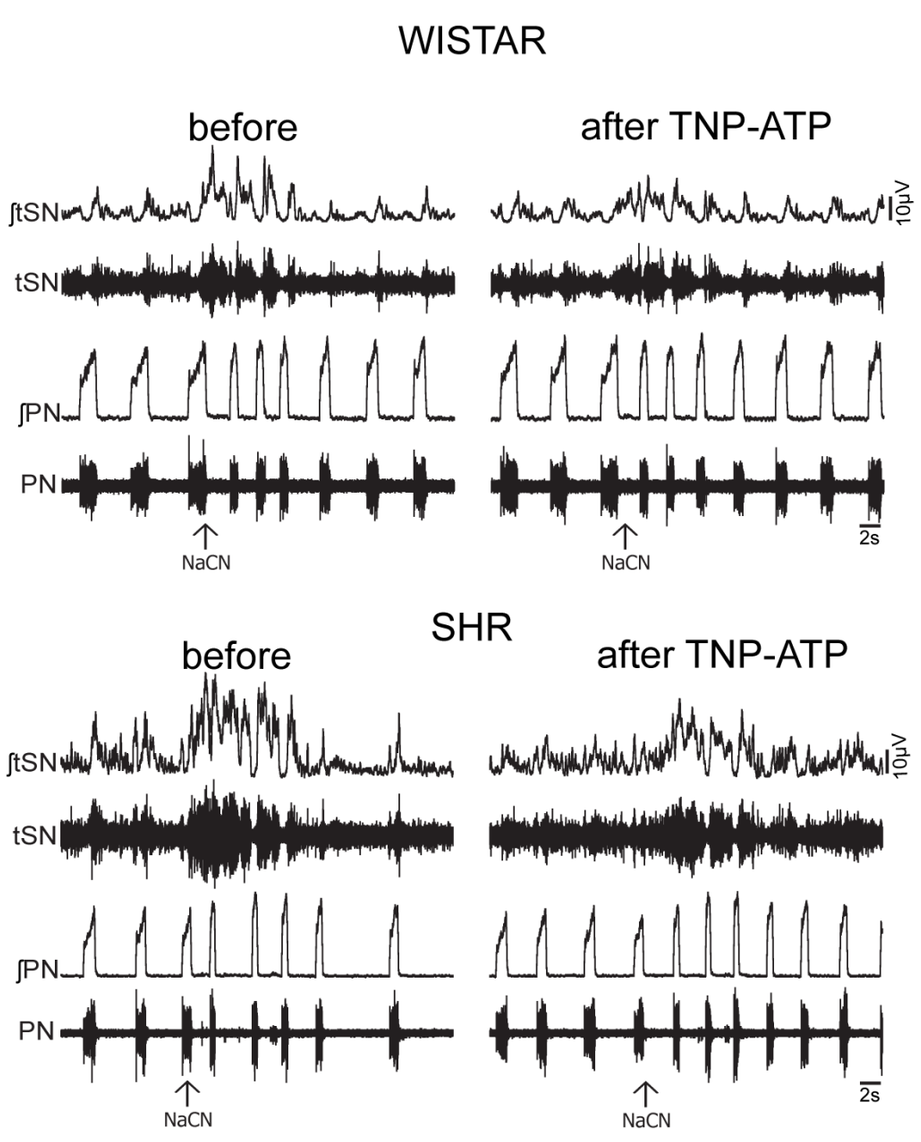

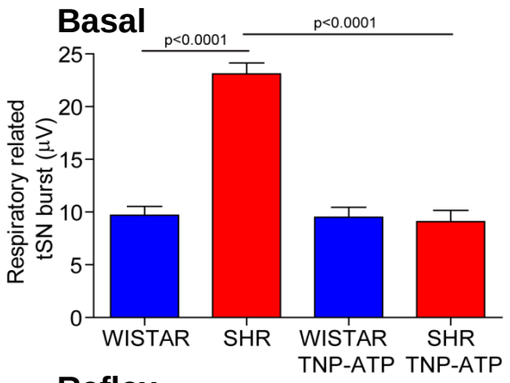

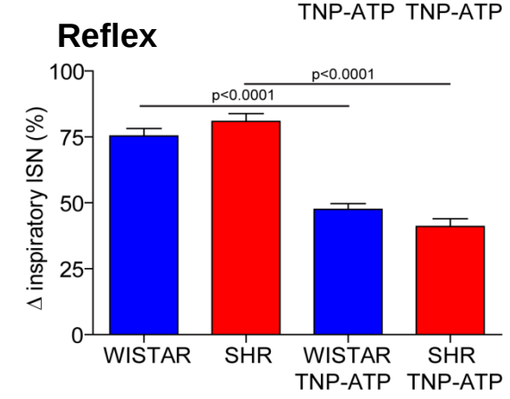

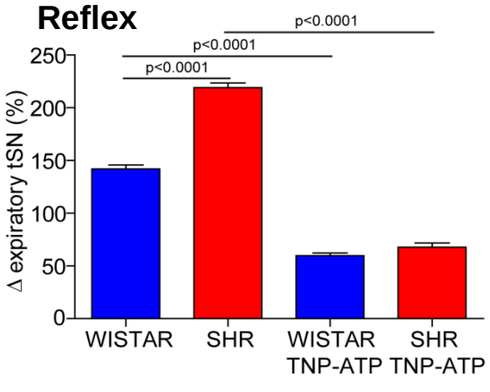

Supplementary Figure 8
Basal and chemoreflex evoked sympathetic activity responses after TNP-ATP (1 μM) microinfused into the carotid body of Wistar and SH rats.
TNP-ATP is a high affinity, non-selective P2X receptor antagonist that inhibits $P2X_1$, $P2X_3$ and heteromeric $P2X_{2/3}$ with a 1000-fold selectivity over $P2X_2$, $P2X_4$ and $P2X_7$ receptors that is structurally distinct to AF-353. These data support the selectivity of AF-353 in blocking P2X3 homomeric and P2X2/3 heterotrimeric receptors rather than non-selective off-target effects. The two reflex bar charts relate to the sympathetic activity that is inspiratory or expiratory modulated.

.

Supplementary Figure 9

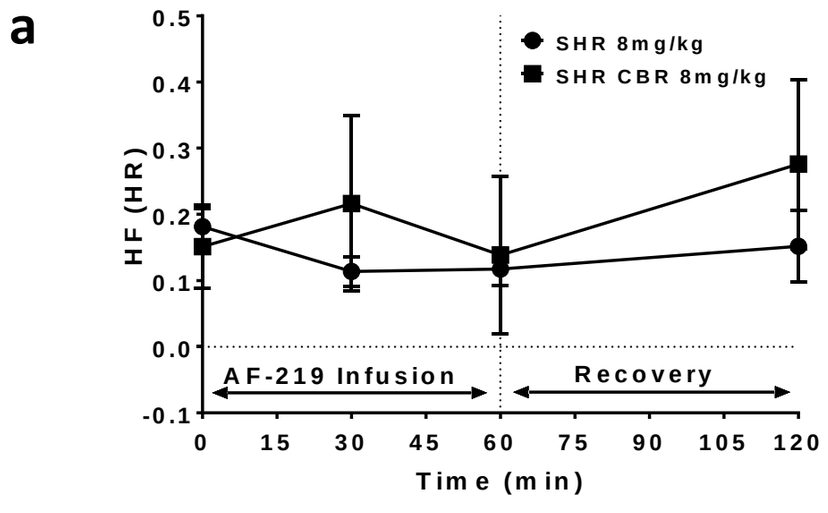

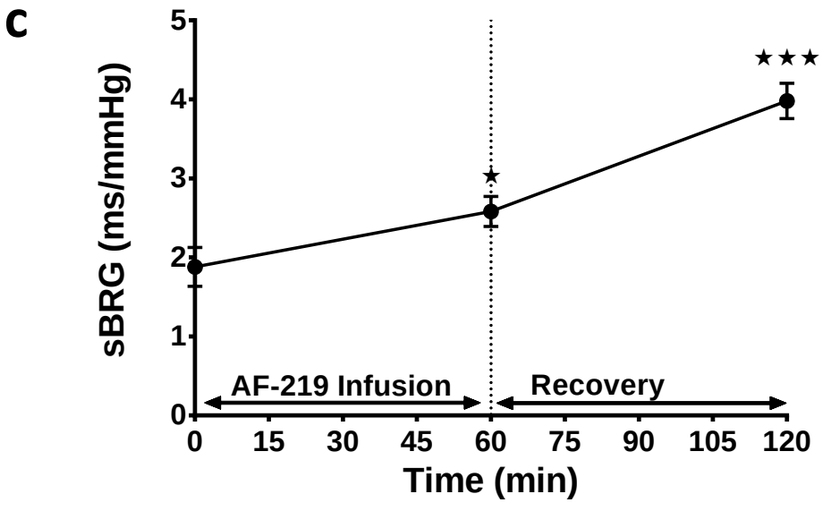

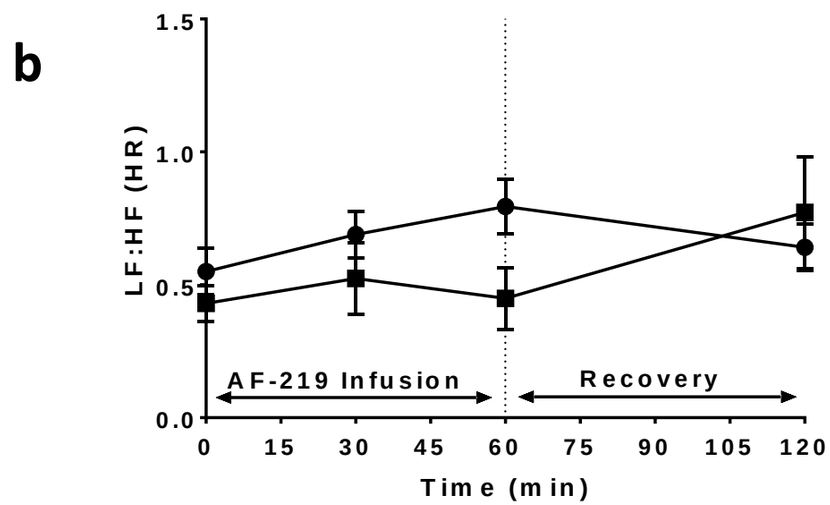

Supplementary Figure 9
Spectral analysis of the heart rate and spontaneous cardiac baroreflex during infusion of AF-219. We found no change in the high frequency spectra (**a**) nor a change in the low to high frequency ratio (LF:HF; (**b**)) following blockade of P2X3 receptors with AF-219 (8 mg/kg/h; *n* = 7). However, there was a significant improvement in the spontaneous baroreceptor reflex gain of heart rate (**c**). * $P < 0.05$, ** $P < 0.01$. One-way ANOVA with Dunnett's test.

Supplementary Figure 10

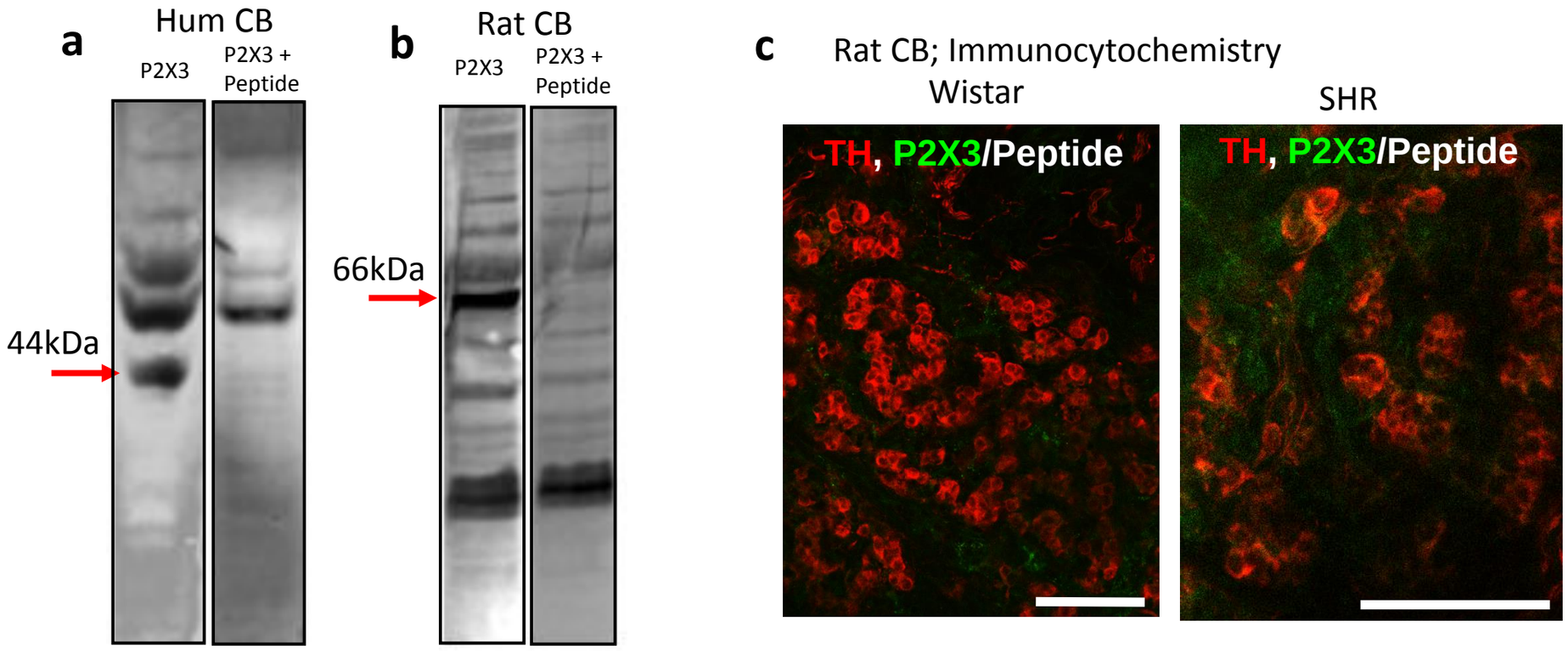

Supplementary Figure 10
P2X3 receptor antibody specificity testing for western blot and immunohistochemistry. Antibody specificity was determined by western blotting on human (Hum; (**a**)) and rat (**b**) carotid bodies (CB). Membranes were incubated with anti-P2X3 antibody in the absence (left lane) or presence (right lane) of the blocking peptide. The absence of the band on the western blot performed in the presence of the blocking peptide revealed that the P2X3 receptor migrates at 44 kDa in human and at 66 kDa in rat. (**c**), the specificity of the P2X3 receptor antibody for immunocytochemistry was tested on CBs from Wistar and SHR using the blocking peptide. No P2X3 receptor immunofluorescence was detected. Glomus cells were identified using tyrosine hydroxylase (TH) immunocytochemistry. Scale bars 100 μm.

Supplementary Figure 11

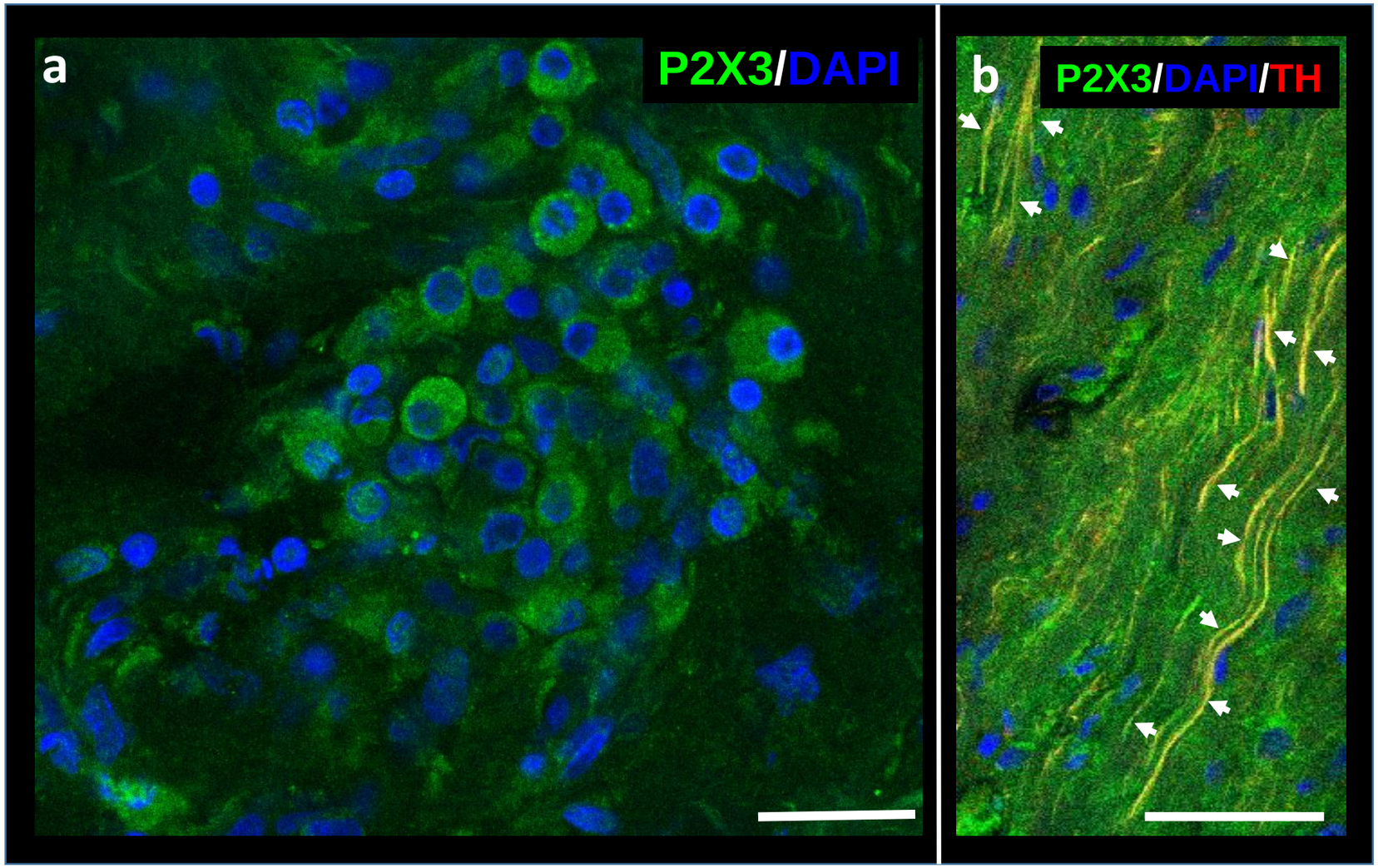

Supplementary Figure 11 P2X3 receptor immunofluorescence within the human carotid body. (**a**) shows P2X3 receptor expression in presumed glomus cells. These data are from a different cadaver to those shown in Fig 6. Scale bar 25 μm. (**b**) Superimposed P2X3, DAPI and tyrosine hydroxylase (TH) immnunofluorescence staining of axons within the CB (examples arrowed) that were immunopositive for P2X3 receptors and TH and appear yellow. These fibres could be petrosal afferents or sympathetic efferents, although the latter is unlikely. Scale bar 50 μm.